Er^{3+},Yb^{3+}:glass-Co^{2+}:$MgAl_2O_4$ diffusion bonded passively Q-switched laser

Yan Zou(邹岩)†, Yong-Ling Hui(惠勇凌), Jin-Lu Cai(蔡瑾鹭), Na Guo(郭娜), Meng-Hua Jiang(姜梦华), Hong Lei(雷訇), and Qiang Li(李强)

Institute of Laser Engineering, Beijing University of Technology, Beijing 100124, *China*

(Received 27 April 2017; revised manuscript received 1 June 2017; published online 11 August 2017)

A Co^{2+}:spinel passively Q-switched erbium-ytterbium-phosphate glass bonded laser pumped at 940 nm is reported. A pulse energy of 210 μJ, a peak power over 70 kW, and beam quality M^2 parameter of 1.2 are obtained under a pump power of 235 mW. An unbonded laser output experiment with the same dimension of the active material and the saturable absorber as the bonded laser output experiment is carried out. The reason why the output in the bonded laser is improved is determined.

Keywords: phosphate glass, passively Q-switched, bonded laser, 940 nm pumped

PACS: 42.55.Xi, 42.60.By, 42.70.Hj **DOI:** 10.1088/1674-1056/26/9/094206

1. Introduction

The laser with a wavelength of 1.5 μm belongs to eye-safe light since it can be absorbed by the eye transparent tissue before reaching the retina. Moreover, it is in the transparency region of the atmosphere. These features make the eye-safe laser an important light source in a wide range of applications, such as in medicine, range-finding, atmospheric sensing, and optical communication.[1–8] Compared with Raman lasers[9] and optical parametric oscillators (OPOs)[10] pumped by high peak power Nd lasers, the laser-diode-pumped Er^{3+},Yb^{3+}:glass-Co^{2+}:$MgAl_2O_4$ passively Q-switched lasers have aroused a great deal of interest due to their compactness, low cost and high reliability. In 2000, Gunnar Karlsson demonstrated a miniature Er:Yb:glass laser that was Q-switched by a Co^{2+}:$MgAl_2O_4$ (Co^{2+}:spinel) saturable absorber for the first time. With a 0.7-mm-thick Co^{2+}:spinel plate, a 2.3 ns pulse wide laser output with peak power exceeding 2 kW was achieved.[11] From then on, a more effective miniature laser with the maximum pulse energy in the shortest pulse width was a major goal for research efforts. Hamlin *et al.*[12] used a Co^{2+}:spinel passive Q-switch to produce 2 nanosecond pulses at a repetition rate from single shot to 20 Hz in 2004, and obtained a nominal pulse energy of 100 μJ, corresponding to a peak power of 50 kW.[12] It is the narrowest pulse width currently. In 2006, Shachkin proposed a special laser resonator which reduced the influence of a thermal lens induced in Er:Yb:glasses and obtained a pulse energy of 1.4 mJ laser output, but the pulse width was 26 ns.[13] Compared with stoichiometric $MgAl_2O_4$ spinels, the alumina-rich spinel exhibits better optical, thermal and mechanical properties. Jiang used an alumina-rich spinel ($Mg_{0.4}Al_{2.4}O_4$) as passive Q-switcher in Er:Yb:glass laser, and obtained a laser output with a pulse energy of 4.8 μJ and a pulse width of 3.5 ns in 2011.[14] Mlynczak and Belghachem,[15] and Mlynczak *et al.*[16] used diffusion bond technique with an Er:Yb:glass and a Co^{2+}:$MgAl_2O_4$ to form a monolithic microchip, and they achieved an output with pulse energy above 32 μJ and pulse width 3.2 ns in the monolithic microchip laser in 2015. Recently, Kigre Inc. presented the MK-2 HEEP microlaser platform, and thereby obtained a pulse energy of 0.2 mJ, corresponding to 5 ns pulse width.[17]

At present, most of passively Q-switched Er:Yb:glass lasers have pulse energies of a few tens of microjoules, and their pulse widths are several nanoseconds. In conventional lasers, the phosphate glass and the spinel crystal are separated. This configuration causes a difficulty in separately aligning the Co^{2+}:spinel and the phosphate glass, leading to an instability of output pulse energy. Furthermore, the length of the cavity is restricted by the arrangement of the active material and the saturable absorber, causing a difficulty in shortening pulse. A diffusion bonded Er:Yb:glass/Co^{2+}:$MgAl_2O_4$ microchip laser presented by Mlynczak *et al.*[15,16] is a way to avoid the disadvantages caused by the separation configuration. However, the pump source wavelength in the microchip laser was 975 nm. The Er:Yb:glass absorption coefficient is sensitive to the wavelength shift around 975 nm,[18] thereby increasing the influence of the operating environment on the output stability.

In this paper, an $Er^{3+}Yb^{3+}$:glass-Co^{2+}:$MgAl_2O_4$ passively Q-switch bonded laser pumped at 940 nm is reported. A peak power of 74 kW with pulse energy 210 μJ and pulse width 2.8 ns is achieved, the beam quality M^2 parameter is obtained to be 1.2. In order to investigate the output characteristics for the Er:Yb:glass/Co:$MgAl_2O_4$ bonded laser and unbonded laser, an unbonded laser output experiment with the

†Corresponding author. E-mail: zouyanofcn@163.com

© 2017 Chinese Physical Society and IOP Publishing Ltd

same dimension of the active material and the saturable absorber as the bonded laser output experiment, is also carried out. The reasons why the output energy is raised, the output pulse width is shortened, and the beam quality in bonded laser is improved, are analyzed theoretically. To the best of our knowledge, the peak power of 74 kW is the highest ever reported for the $Er^{3+}Yb^{3+}$:glass-Co^{2+}:$MgAl_2O_4$ passively Q-switch laser pumped at 940 nm, and the reasons for changing the output characteristics resulting from diffusion bonding are analyzed.

2. Experiment setup

The scheme of the Er:Yb:glass/Co:$MgAl_2O_4$ bonded/unbonded laser is shown in Fig. 1. The phosphate glass in the bonded/unbonded laser was provided by Shanghai Institute of Optics and Fine Mechanics (SIOM), China, and the optical quality of the phosphate glass in both lasers were the same. In order to reduce the reabsorption loss and up-conversion process, the concentrations of the erbium and ytterbium ions in phosphate glass were 1 wt.% and 21 wt.%, respectively. The small signal transmission of saturable absorbers was chosen to be 80%.

The Er:Yb:glass/Co:$MgAl_2O_4$ bonded crystal was obtained with the diffusion bonding technique, and the bonding process was completed in Beijing University of Technology. Diffusion bonding of an Er:Yb:glass with Co:$MgAl_2O_4$ involved precision polishing, assembly by optical contacting, and heat treatment. After the procedures, the Er:Yb:glass-Co:$MgAl_2O_4$ bonded crystal was achieved. The imaging of the bonding interface was taken with a high resolution transmission electron microscopy (HRTEM). From the image, no defect was observed on the interface. It proved that the bonding process was finished successfully. Compared with the internal losses of separated phosphate glass and spinel, the internal loss of the material remained unchanged. The bonded crystal and the image of bonding interface are shown in Figs. 2(a) and 2(b).

By cutting and polishing, the phosphate glass-spinel bonded crystal used in the experiment was obtained, as shown in Fig. 2(c). In the experiment, the cross section for the bonded crystal was 1 mm × 1 mm, the length of the phosphate glass part was equal to 3 mm, the length of the spinel part was equal to 1.6 mm, so the total length of the bonded crystal was 4.6 mm. The bonded crystal was fixed by a small holder, and placed between the rear mirror and the output mirror as shown in Fig. 3. In the unbonded laser, the dimensions of the separate phosphate glass and spinel were equal to those of the phosphate glass part and the spinel part, respectively. So the phosphate glass dimension was 1 mm × 1 mm × 3 mm, and the spinel dimension was 1 mm × 1 mm × 1.6 mm. Similarly, the separate phosphate glass and spinel were fixed by two small holders, and placed between the rear mirror and the output mirror.

A TO-3 packed diode laser with a beam waist radius of 200 μm, operating at 940 nm at room temperature (25°C) was used to longitudinally pump the active material, whose output is shown in Fig. 4. Compressed and focused, the pump light was assumed to be a small circular beam near the focal point. The pump beam waist in the active material was 75 μm, by optimizing the output properties, it was located at 0.5 mm behind the pump face. In the experiment, the pump period was 7 ms and the frequency of pumping was 10 Hz. A plane-parallel resonator was used here, and the active material-saturable absorber bonded/unbonded component was located between the rear mirror and output coupler. The rear mirror had a high transmission at 940 nm and a high reflection at 1535 nm. The output mirror was characterized by partial transmission (T = 10 %) at 1535 nm. The length of the resonator was equal to 5 mm.

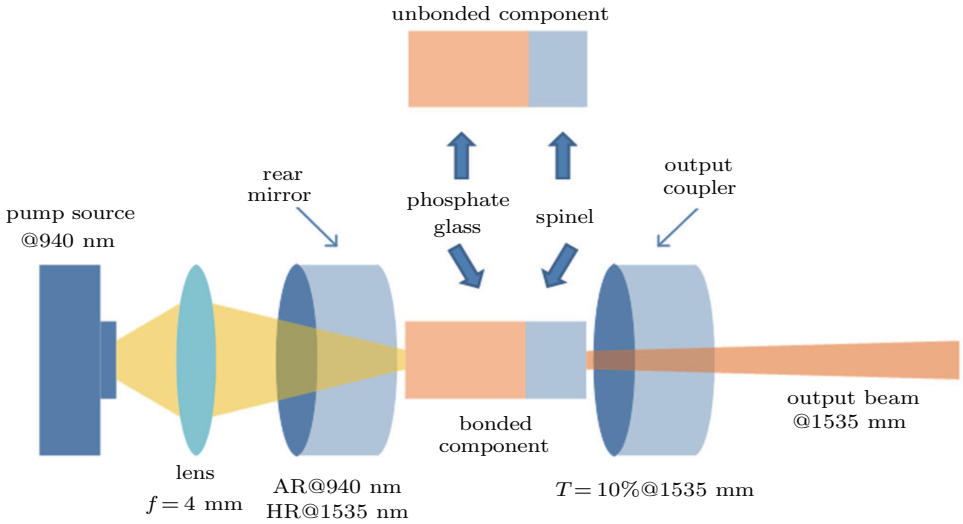
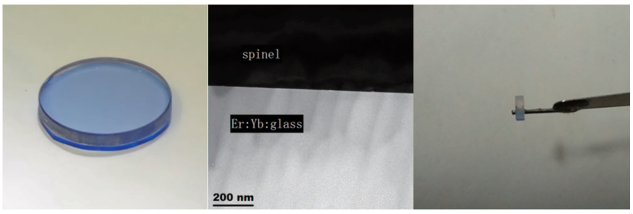


Fig. 1. (color online) Schematics of the bonded/unbonded laser experiment.



(a) (b) (c)

Fig. 2. (color online) (a) The Er:Yb:glass-Co:$MgAl_2O_4$ bonded crystal; (b) high-resolution transmission electron microscopic image of bonding interface; (c) bonded crystal used in the experiment.

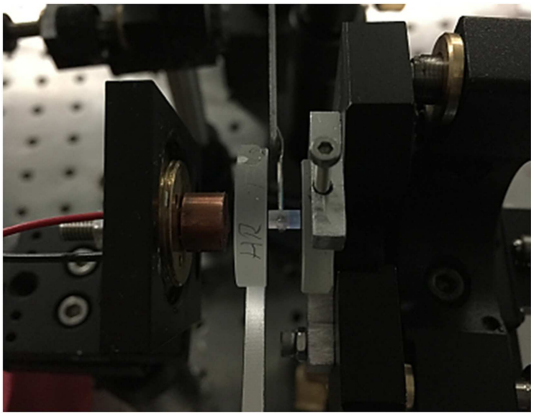


Fig. 3. (color online) Fixed Er:Yb:glass-spinel bonded crystal and the bonded laser setup.

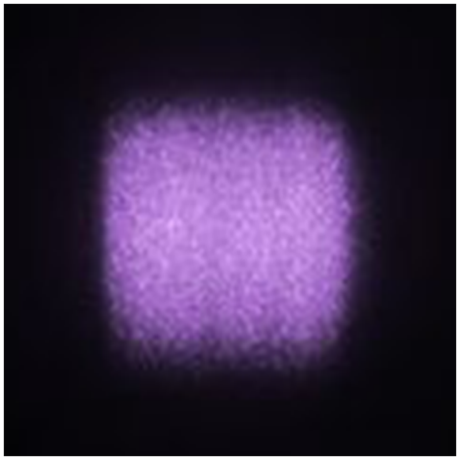


Fig. 4. (color online) Pump light pattern from the TO-3packeddiodelaser.

In the case of the bonded component, the phosphate glass was diffusion bonded by a Co:spinel, and the total length of the diffusion bonded material was 4.6 mm. The antireflection coatings at 940 nm (AR@940 nm) and 1535 nm (AR@1535 nm) were coated on the side near the rear mirror. The high reflection coatings at 940 nm (HR@940 nm) and antireflection coatings at 1535 nm (AR@1535 nm) were coated on the side near the output coupler. The spaces for rear mirror-bonded component and bonded component-output coupler were both nearly 0.1 mm.

In the case of the unbonded component, the phosphate glass and the Co:spinel were separated. For the active material, antireflection coatings at 940 nm (AR@940 nm) and 1535 nm (AR@1535 nm) were coated on the side near the rear mirror. For the saturable absorber, the side near the output coupler was coated by high reflection coating at 940 nm (HR@940 nm) and antireflection coating at 1535 nm (AR@1535 nm). Other sides of the component had no coating. The spaces for rear mirror-active material, active material-saturable absorber, and saturable absorber-output coupler were all nearly 0.1 mm.

3. Experiment results

The results of pulses generated from the bonded laser and the unbonded laser are shown in Figs. 5 and 6. By measuring the output with a power meter and an energy meter, the average output power grows with increasing the average pump power, but the output pulse energy is changed slightly. With average pump power reaching a maximal value of 235 mW, the output characteristics are achieved for each component. The maximum average output power of bonded component is 11.54 mW, and the pulse energy is 210 μJ. The maximum average output power of unbonded component was 3.4 mW, corresponding to 70 μJ pulse energy. The optical-to-optical efficiency of 4.9% is achieved in bonded component, which is three times higher than that of unbonded component (1.4%). Compared with the power threshold of 120 mW in unbonded component, the power threshold in bonded component was 90 mW.

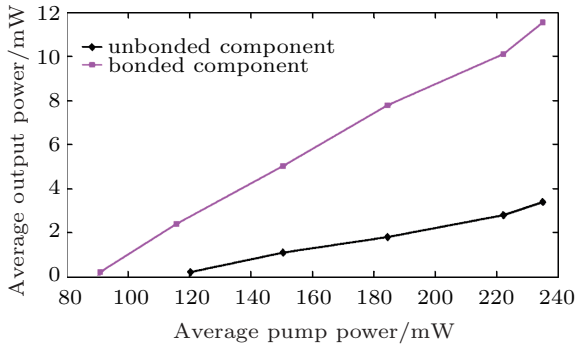


Fig. 5. (color online) Average output powers versus average pump power for the bondedand the unbonded component.

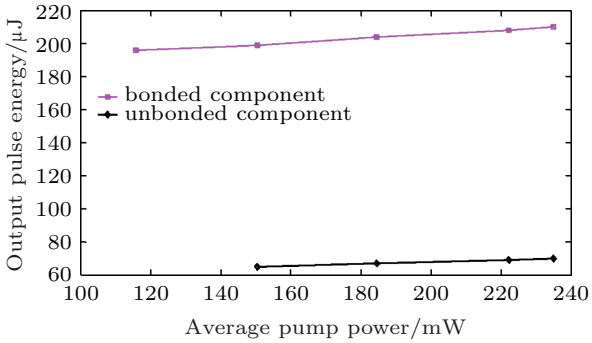


Fig. 6. (color online) Output pulse energies versus average pump power for the bonded and the unbonded component.

The output pulse repetition rates of the output for the bonded component and the unbonded component are shown in Figs. 7 and 8. Above threshold, the repetition rate of the output pulse increases approximately linearly with average pump power increasing. Under an average pump power of 235 mW, the pulse repetition rate of the output for the bonded component is 990.3 Hz, and that of the unbonded component is 803.7 Hz.

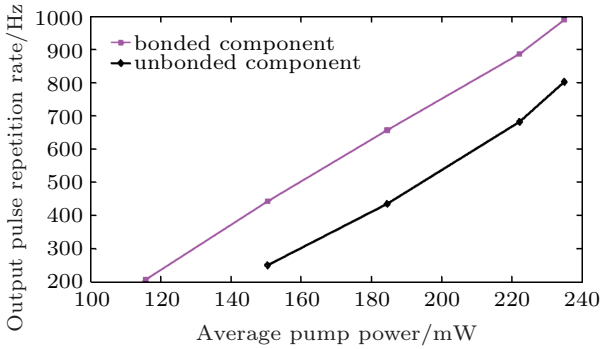


Fig. 7. (color online) Output pulse repetition rates versus average pump power for the bonded component and the unbonded component.

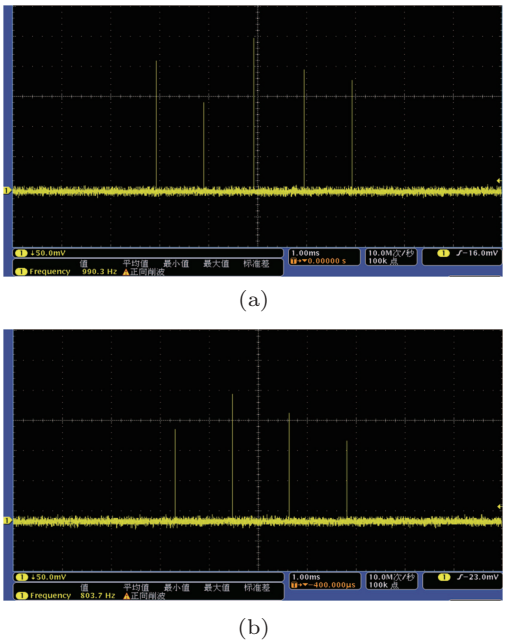


Fig. 8. (color online) Output pulse repetition rates of (a) bonded component (b) unbonded component.

The output pulse widths for the bonded and unbonded component are shown in Figs. 9 and 10. With the average pump power increasing, the output pulse width changes very little for both the bonded and unbonded component. Under the average pump power of 235 mW, the pulse widths are equal to 2.82 ns in the bonded component and 6 ns in the unbonded component, respectively. Considering the pulse energy mentioned above, the peak power of the bonded component is 74 kW, and the peak power of the unbonded component is 12 kW. It should be noticed that the peak power in the bonded component is six times higher than that of the unbonded component.

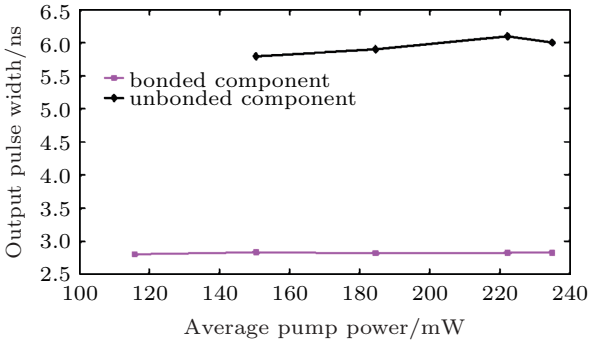


Fig. 9. (color online) Output pulse widths versus average pump power for the bonded and the unbonded component.

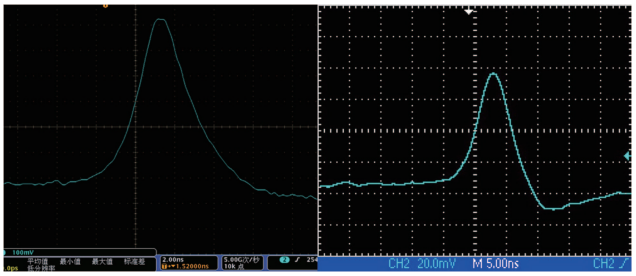


Fig. 10. (color online) Output pulse widths of (a) bonded and (b) unbonded component.

Based on the knife-edge measuring method, the M^2 parameter (average of M^2x and M^2y) of the bonded component is 1.2 and that obtained from the unbonded component is 1.3. The beam quality in bonded component is slightly better than that of the unbonded component. The beam quality for the bonded component and that for the unbonded component are both shown in Fig. 11.

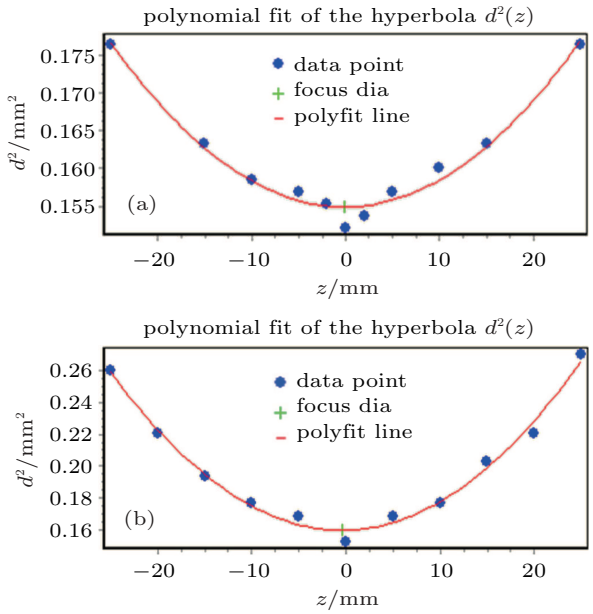


Fig. 11. (color online) Beam quality measurement curves for (a) bonded and (b) unbonded component.

4. Discussion

As can be seen from the above, the output pulse energy of the bonded component is much higher than that of the unbonded component, and the output pulse width of the bonded component is shorter than the other's. In addition, the beam quality for the phosphate glass/Co:spinel component is better after diffusion bonding.

In reviewing the phosphate glass-spinel bonded/unbonded component used in experiments, it is clear that two changes take place. Firstly, the thermal conductivity of spinel is much higher than that of the phosphate glass (Spinel: 25 W/m·K), phosphate glass : 0.745 W/m·K). Adding a spinel for the phosphate glass as a heat sink by diffusion bonding improves the laser component thermomechanical properties, resulting in the thermal effect of laser components changing. Secondly, using the diffusion bond technique with the phosphate glass and the spinel reduces the Fresnel losses on surfaces. So the internal loss in bonded component is much smaller than that in unbonded component. According to the two considerations above, we discuss the influence of diffusion bonding on the laser output.

4.1. Laser output improvements caused by thermomechanical property change

In order to clarify the thermal effects in the bonded/unbonded lasers, the temperature distributions, stress distributions and the deformation of materials are estimated by finite element method (FEM). In the simulation, two modules are defined. One named the bonded module is formed by an Er:Yb:glass which is diffusion bonded with a Co:spinel saturable absorber. The other named the unbonded module is formed by an Er:Yb:glass and a Co:spinel, the two parts are separated. Because the thermal conductivity of spinel is much higher than that of phosphate glass, the heat deposition in spinel is ignored. Therefore, only the phosphate glass is considered in the simulation. The bonded module and unbonded module are shown in Figs. 12(a) and 12(b). The dimensions and property parameters of the phosphate glass and the spinel used here are detailed in Table 1.

A study of thermal effect first requires the calculation of the temperature value at any position of material. If we assume that the pump beam propagates along the z-axis and for the simplification we make an assumption that the pump beam on the end face of material has a Gaussian intensity profile with pump beam radius ω_{p}, then any point temperature $T(x,y,z,t)$ can be solved by[19,20]

$$\rho C_{\mathrm{p}} \frac{\partial T(x,y,z,t)}{\partial t} - K_{\mathrm{c}} \nabla^2 T(x,y,z,t) = \xi \alpha_{\mathrm{p}} \frac{2P_{\mathrm{p}}}{\pi \omega_{\mathrm{p}}^2} \exp\left[-\frac{2\left(x^2+y^2+z^2\right)}{\omega_{\mathrm{p}}^2} - \alpha_{\mathrm{p}} z\right], \quad (1)$$

where ρ is the density, C_{p} is the specific heat, K_{c} is the thermal conductivity, ξ is the fraction of absorbed pump power converted into heat, α_{p} is the absorption coefficient, P_{p} is the incident pump power, and T is the temperature.

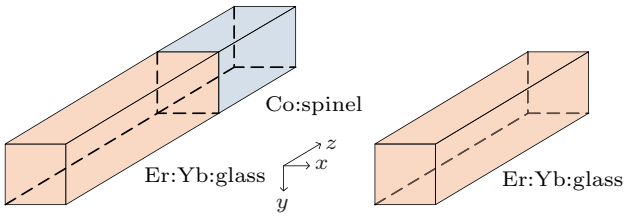


Fig. 12. (color online) Er:Yb:glass-Co:spinel modules in the simulation: (a) bonded module and (b) unbonded module.

Table 1. Material propertis of Er:Yb:phosphate glass and Co:spinel crystal.[22–25]

Parameters	Symbols / unit	Er:Yb:glass	Co:spinel
Material cross section	$l \times l$ / mm*mm	1×1	1×1
Material length	L/mm	3	1.6
Young's modulus	E/pa	70×10^9	276×10^9
Poisson's ratio	ν	0.24	0.26
Density	ρ/kg·m^{-3}	2633	3577
Refractive index	n_0	1.53	1.69
Temperature coefficient of the refractive index	dn/dT/K^{-1}	-1×10^{-6}	9×10^{-6}
Specific heat	C_{p}/J·kg^{-1}·K^{-1}	840	819.1
Thermal conductivity	K/W·m^{-1}·K^{-1}	0.745	25
Thermal expansion coefficient	α_{T}/K^{-1}	7.2×10^{-6}	6.97×10^{-6}
Piezo-optic coefficient	π/ Pa^{-1}		$\pi_{11} = 2.693 \times 10^{-13}$
			$\pi_{12} = -3.3103 \times 10^{-13}$
			$\pi_{44} = 5.908 \times 10^{-13}$
Elasto-optic coefficient	p	$p_{11} = 0.2842$	
		$p_{12} = 0.311$	
		$p_{44} = -0.0134$	
Absorption coefficient at 940 nm	α_{p}/cm^{-1}	4.28	
Heat generation ratio	ξ	0.3876	
Pump size radius	ω_{p}/μm	75	

In the laser operation simulation, the pump period is 7 ms and a duty-cycle 7% is used. The frequency of pumping is 10 Hz, which is much greater than the inverse of the thermal relaxation time, i.e.,[21]

$$\frac{1}{\tau_{\mathrm{p}}} = \frac{4K_{\mathrm{c}}}{c_{\mathrm{p}}\rho r_0^2}, \tag{2}$$

where r_0 is the active material radius. In this case, the differential equation (1) is solved in steady-state condition.

For the boundary conditions, the initial temperatures of active material and saturable absorber both equal ambient temperature 293 K. As shown in Fig. 3, the active material-saturable absorber in bonded laser is fixed by a small holder. The holder is so small that the influence on the thermal effect of bonded crystal could be ignored. Similarly, the separate active material and saturable absorber are fixed on two small holders in unbonded laser, the influences of holders on the thermal effect are also ignored. Based on the treatment above, all the external faces of bonded module and unbonded module are subjected to nature convection. To show the thermal effects of modules under each pump power, different average pump powers between 100 mW and 200 mW are used here.

Figure 13 displays exemplary solutions for the bonded module and the unbonded module under an average pump power of 200 mW. A comparison between the two modules shows that the diffusion bonded spinel has very little influence on the temperature distribution for the phosphate glass since it is far from the pumping face. As to the stress distribution, the stress maximum values appearing on the pump face for the bonded module and the unbonded module are close to each other. However, the stress minimum value in bonded module is three percent of that in unbonded module. For the deformation of material, the maximum deformation of pumping face in the bonded module is close to that of the unbonded module. However, the deformation of the output face in the bonded module is much less than that of the unbonded module. As a conclusion, the stress minimum values of material and the deformations of the output face in the two modules are different under a similar temperature distribution. The reason for the differences in the stress distribution and the end face deformation is as follows. As shown in Fig. 13, the stress minimum value of material and the deformation of the output face in bonded module are on the spinel part. The spinel is much harder than the phosphate glass, and the thermal expansion coefficient of spinel is smaller than that of phosphate glass.

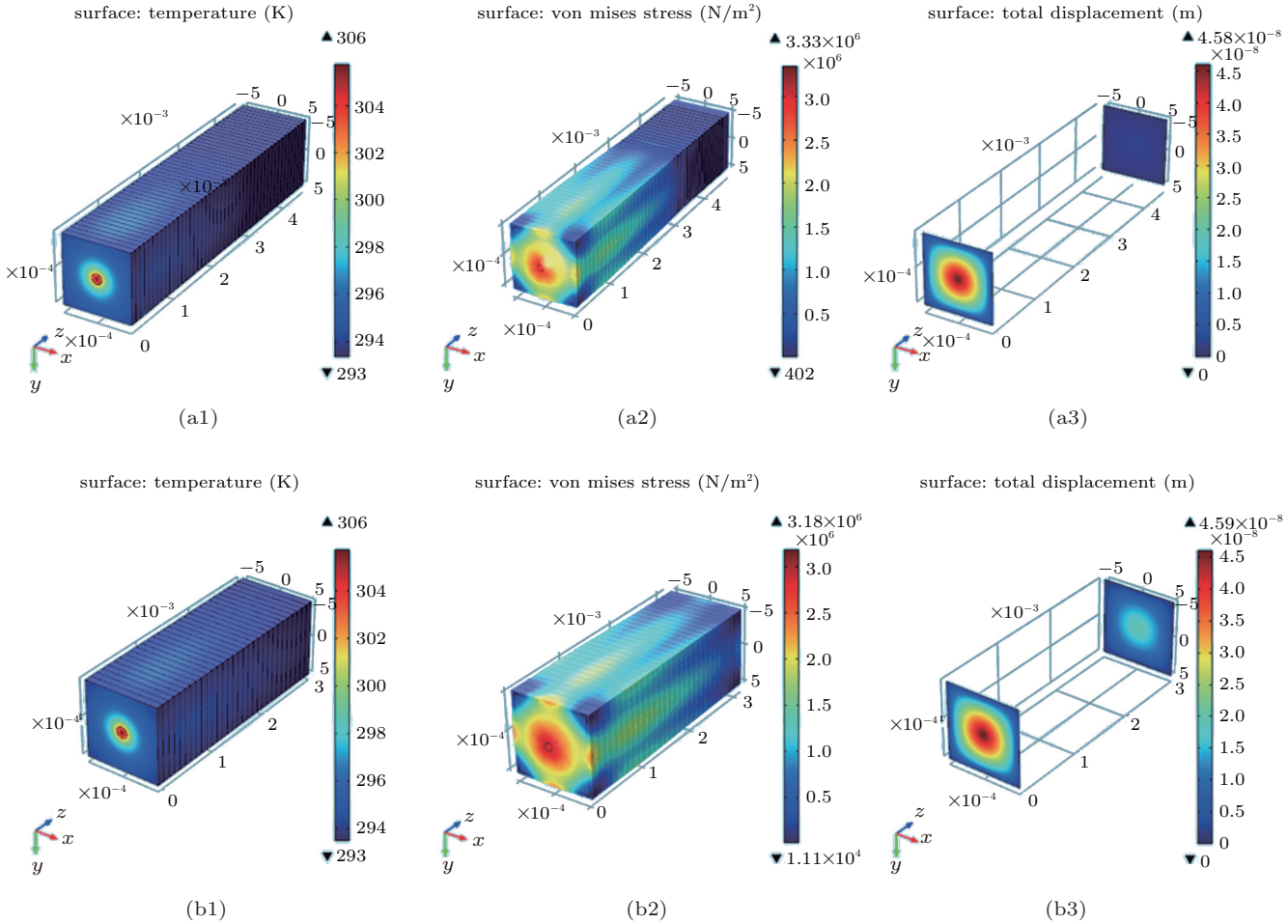


Fig. 13. (color online) Temperature distributions, von Mises stresses, and end face deformations of(a1,a2,a3) bonded module and(b1,b2,b3) unbonded module, under average pump power 200 mW.

When the temperature in material rises, the thermal expansion of spinel will be much weaker than phosphate glass. Thus, the stress and deformation induced by thermal expansion in spinel will be much smaller than those of phosphate glass. Due to the spinel part in bonded component, the stress and deformation of the bonded component are both different from those of the unbonded component evidently.

After simulating with other pump powers, the similar appearances of temperature distribution, von Mises stress and end face deformation are also found in modules.

Concerning the wavefront distortion induced by thermal effect, the change of the optical path length for the beam passing through the laser active material is given by the change of refractive index with temperature, the end face deformation and the thermally induced birefringence. The overall optical path difference (OPD) is expressed as[26]

$$\mathrm{OPD}(x,y) = \frac{\partial n}{\partial T}\int_0^L T(x,y,z)\,\mathrm{d}z + (n_0-1)\,\Delta L(x,y) + \sum_{i,j=1}^{3}\frac{\partial n}{\partial \sigma_{ij}}\int_0^L \sigma_{ij}(x,y,z)\,\mathrm{d}z, \tag{3}$$

where L is the length of material along the beam propagation path and n_0 is the refractive index of material under room temperature.

For the bonded and the unbonded module, their OPD can be written as

$$\mathrm{OPD}_{\text{bonded module}} = \mathrm{OPD}_{\text{phosphate glass}} + \mathrm{OPD}_{\text{spinel}}, \tag{4}$$

$$\mathrm{OPD}_{\text{unbonded module}} = \mathrm{OPD}_{\text{phosphate glass}}. \tag{5}$$

Then, the OPD is expressed in a Taylor series as follows: [27]

$$\mathrm{OPD}(s) = p_0 + p_1 s + p_2 s^2 + p_3 s^3 + \cdots + p_n s^n, \tag{6}$$

where p_n is the coefficient of the polynomial, the focal length of the thermal lens f_{thermal} is determined by the quadratic part of the OPD(s) function as

$$f_{\text{thermal}} = -\frac{1}{2p_2}. \tag{7}$$

Figure 14 shows the results of the estimated thermal focal length versus the average pump power for the bonded module and the unbonded module. We can see that the thermal focal length of the bonded module is almost twice that of the unbonded module at each pump power. Namely, using the diffusion bond technique for the phosphate glass and the spinel can greatly reduce the thermal effect.

It is clear that the decrease of thermal effect provides a better beam quality. This is the reason why the beam quality of the output becomes slightly better after diffusion bonding.

On the other hand, the decrease of thermal effect provides a better spatial match between the pump beam and the output beam, which may be a factor for raising the output pulse energy. In general, the degree of overlap between the fundamental TEM_{00} modes of the resonator and the pump beam, η_{B}, is defined as[28]

$$\eta_{\mathrm{B}}(z) = \frac{4\omega_{\mathrm{p}}^2(z)\,\omega_{\mathrm{o}}^2(z)}{\left(\omega_{\mathrm{p}}^2(z)+\omega_{\mathrm{o}}^2(z)\right)^2}, \tag{8}$$

where $\omega_{\mathrm{p}}(z)$ and $\omega_{\mathrm{o}}(z)$ are the spot radii of the pump beam and the fundmental output beam. In the longitudinal pump configuration, the absorption of the pump beam in the active material is usually assumed to be the Lambert law pattern. Hence, the exponential absorption of Er:Yb:glass for pump light causes a nonuniform gain distribution along the longitudinal axis of the active material. The relationship between the pump power intensity and the phosphate glass length is shown in Fig. 15.

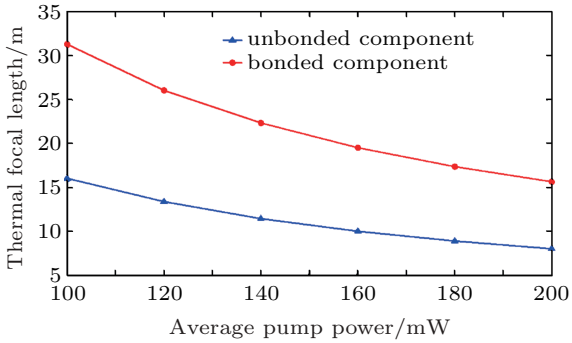


Fig. 14. (color online) Thermal focal lengths versus average pump power for the bonded/unbonded module under different pump powers.

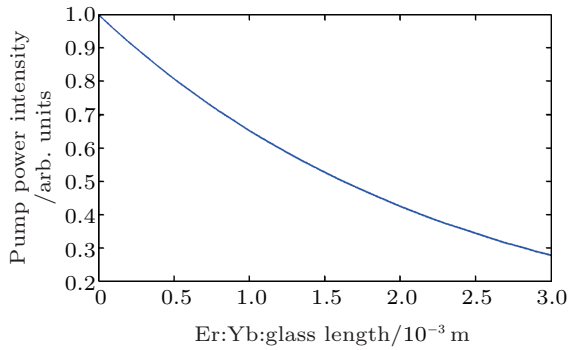


Fig. 15. (color online) Variation of pump power intensity with the length of Er:Yb:glass.

When the pump light propagation length is 1.5 mm, the pump power intensity falls to half of its maximum value approximately. We assume that the first half of the phosphate glass (from the pump face to the mid-point of the material length, i.e., at the position of 1.5 mm) makes a major contribution to the laser output and use the average pump beam radius $\overline{\omega_{\mathrm{p}}}$ and the average output beam radius $\overline{\omega_{\mathrm{o}}}$ in this range to estimate the beam overlap efficiency η_{B}.

The pump light could be regarded as a circular beam in a short distance after focusing, and the divergence is estimated to be 0.0052 rad. According to the following equation:[29]

$$\omega_{\mathrm{p}}(z) = \omega_{\mathrm{p0}} + \theta_{\mathrm{p}}|z|, \tag{9}$$

the average pump beam radius $\overline{\omega_p}$ is obtained to be about 75.14 μm.

The effective thermal lens in end-pumped lasers is close to the surface of the pumping end.[30] Taking average pump power to be 200 mW for example, we assume that the effective thermal lens is located at a distance of 0.4 mm behind the pump face, where the temperature is highest along the z-axis. After calculating, the average output beam radii are 32.12 μm for the bonded component and 31.54 μm for the unbonded component, respectively. So the values of beam overlap efficiency η_B are 52.26% for the bonded component and 50.95% for the unbonded component, respectively. The beam overlap efficiency in the bonded component is only a few percent higher than that of the unbonded component. Thus, the decrease of thermal effect after diffusion bonding plays a limited role in raising the output pulse energy.

4.2. Laser output improvements caused by internal loss change

In the Q-switched laser operation, an expression for the laser output pulse energy is derived as[31]

$$E_o = \frac{h\nu A}{2\sigma\gamma}\ln\left(\frac{1}{R}\right)\ln\left(\frac{n_i}{n_f}\right), \tag{10}$$

where $h\nu$ is the output photon energy, A is the cross-sectional area of the output, σ is the stimulated emission cross section of active material, γ is an inversion reduction factor, R is the output mirror reflectivity, n_i and n_f are the initial and final population inversion densities of saturable absorber.

Now define the parameter n_f/n_i as[32]

$$\frac{n_f}{n_i} = 1 + N\ln\left(\frac{n_f}{n_i}\right) - \frac{1}{\alpha}(1-N)\left[1-\left(\frac{n_f}{n_i}\right)^{\alpha}\right], \tag{11}$$

where

$$N = \frac{\delta\ln\left(1/T_0^2\right) + \ln(1/R) + L}{\ln\left(1/T_0^2\right) + \ln(1/R) + L},$$

$\alpha = \sigma_{gs}/\gamma\sigma$, $\delta = \sigma_{es}/\sigma_{gs}$, and $L = 2\alpha_{sc}(l + l_s)$, with T_0 being the small signal transmission of Co:spinel, L the internal loss per round trip, σ_{gs} the Co^{2+} ground state absorption cross-section at the lasing wavelength, σ_{es} the Co^{2+} excited state absorption cross-section at the lasing wavelength, α_{sc} the scattering loss, l the length of phosphate glass, and l_s the length of saturable absorber.

Under a pump power of 200 mW, the typical parameters above are follows:[33] $\sigma = 7.5\times10^{-25}\text{m}^2$, $\gamma = 2$, $\sigma_{gs} = 3.5\times10^{-23}\text{m}^2$, $\sigma_{es} = 1.0\times10^{-24}\text{m}^2$, $\alpha_{sc} = 0.002\ \text{cm}^{-1}$, $R = 90\%$, $T_0 = 80\%$, and $A = 2.642\times10^{-9}\text{m}^2$. Owing to Fresnel losses on surfaces, the internal loss per round trip is simplified into $(1-0.95^2)$ for the bonded component and $(1-0.95^4)$ for the unbonded component. Substituting these parameters into Eqs. (10) and (11), the output pulse energies of 59 μJ in bonded component and 36 μJ in unbonded component for the fundamental TEM_{00} mode are obtained, respectively. Obviously, the laser output from the bonded component is about sixty percent higher than that of the unbonded component. If we consider the higher order modes in the cavity and the optimization of the pump distribution in the active material, the output pulse energy for the bonded component would be much higher than that of the unbonded component.

To verify the influence of the internal loss on the output pulse energy, an experiment of the unbonded components with all end faces coatings is designed. In this experiment, the dimensions of phosphate glass and spinel are equal to those of the previous unbonded laser, all the end faces of phosphate glass and spinel are coated by antireflection coatings at 1535 nm (AR@1535 nm). Under the same pump condition as that of the previous unbonded laser, the maximum output pulse energy in this experiment is 193 μJ. The output pulse energy of 193 μJ is much higher than that of previous unbonded laser, but lower than that of the bonded laser. The reason for the change of the output pulse energy is assumed to be that, on one hand, the less Fresnel loss makes a great contribution to the output pulse energy; on the other hand, the cavity loss introduced by the separate configuration misalignment tolerance makes the output energy lower than that of the bonded laser.

Besides, the less internal loss leads to inversion population density increasing. Under the conditions of the short cavity length and the fast Q-switched operation, the output pulse width of the bonded component would be shorter than that of the unbonded component. Considering the output pulse energy, the peak power of the bonded component is higher than that of the unbonded component distinctly.

In summary, the weaker thermal effect in the bonded component has an improvement in the output beam quality and a limited contribution to the raising of the output pulse energy. The less internal loss due to diffusion bonding in the bonded component plays an important role in elevating the output power. Meanwhile, it resulted in a shorter pulse width in the bonded component.

5. Conclusions

A Co^{2+}: spinel passively Q-switched erbium-ytterbium-phosphate glass bonded laser pumped at 940 nm is reported. A pulse energy of 210 μJ at a pulse width of 2.8 ns is achieved, corresponding to the peak power of 74 kW. Compared with the unbonded laser, the bonded laser has an output three times the output pulse energy of unbonded laser, the beam quality of the bonded laser is slightly better, and the pulse width of it is shorter clearly. The reasons for the improvement of the output are analyzed. The decreasing of thermal effects in bonded laser is the reason for the improvement of beam quality. The

less internal loss is the major contribution to the output pulse energy, and makes the output pulse width shortened.

The thermal analysis for the bonded/unbonded laser indicates that the spinel has very little influence on the phosphate glass because it is bonded on the back face of the phosphate glass. If the spinel is bonded on the pump face of the phosphate glass, the spinel would have an effective cooling on the active material, so the thermal effects of the active material would be much weaker. Another effective way to reduce the thermal effect of the active material is to use active cooling in lasers. In the experiments above, the bonded/unbonded components are fixed by small holders, and no special cooling method is used. If the components are mounted on heat sinks which could be cooled to lower temperature, the thermal effects of the active material will be weaker further. As a result, the repetition rate of the pump light can be increased, and the average power of output will be higher and has good beam quality as well.

References

[1] Chen Y J, Lin Y F, Zou Y Q, Luo Z D and Huang Y D 2013 *Laser Physics Letters* **10** 095803

[2] Zhang H N, Li P, Wang Q P, Chen X H, Zhang X Y, Chang J and Tao X T 2014 *Applied Optics* **53** 7189

[3] Starodubov D, McCormick K and Volfson L 2015 *SPIE Defense+ Security. International Society for Optics and Photonics* p. 946104-1

[4] Silver M, Lee S T, Borthwick A, Morton G, McNeill C, McSporran D, McRae I, McKinlay G, Jackson D and Alexander W 2016 *SPIE Defense+ Security. International Society for Optics and Photonics* p. 98320R-1

[5] Shumpei K, Takeshi S, Yojiro W, Toshiyuki A, Kimio A, Hisamichi T, Takayuki Y, Yoshihito H and Hamaki I 2012 *SPIE Asia-Pacific Remote Sensing. International Society for Optics and Photonics* p. 85260E-1

[6] Steinvall O, Persson R, Berglund F, Gustafsson O and Gustafsson F 2014 *SPIE Defense+ Security. International Society for Optics and Photonics* p. 90800W-1

[7] Zhang X, Diao W F, Liu Y, Zhu X P, Yang Y, Liu J Q, Hou X and Chen W B 2014 *Appl. Opt.* **53** 2465

[8] Yu H H, Wang S X, Han S, Wu K, Su L B, Zhang H J, Wang Z P, Xu J and Wang J Y 2014 *Opt. Lett.* **39** 1341

[9] Murray J T, Powell R C, Peyghambarian N, Smith D, Austin W and Stolzenberger R A 1995 *Opt. Lett.* **20** 1017

[10] Agnesi A, Dell'Acqua S and Reali G 2000 *Appl. Phys. B* **70** 751

[11] Karlsson G, Pasiskevicius V, Laurell F, Tellefsen J A, Denker B, Galagan B I, Osiko V V and Sverchkov S 2000 *Appl. Opt.* **39** 6188

[12] Hamlin S J, Hays A D, Trussell C W and King V 2004 *Proceedings of SPIE* **5332** 97

[13] Shachkin L V 2006 *Quantum Electronics* **36** 106

[14] Jiang D P, Zou Y Q, Su L B, Tang H L, Wu F, Zheng L H, Li H J and Xu J 2011 *Laser Physics Letters* **8** 343

[15] Mlynczak J and Belghachem N 2015 *Optics Communications* **356** 166

[16] Mlynczak J, Belghachem N, Kopczynski K, Kisielewski J, Stepien R, Wychowaniec M, Galas J, Litwin D and Czyzewski A 2016 *Quantum Electronics* **48** 1

[17] http://www.kigre.com/products/mk2.html

[18] Trussell C W, King V, Hays A D, Hutchinson J A and Hamlin S J 2004 *Advanced Solid-State Photonics Presentation*

[19] Chénais S, Druon F, Forget S, Balembois F and Georges P 2006 *Progress in Quantum Electronics* **30** 89

[20] Hardman P J, Clarkson W A, Friel G J, Pollnau M and Hanna D C 1999 *IEEE Journal of Quantum Electronics* **35** 647

[21] Koechner W 2006 *Solid-state Laser Engineering*, 6th edn. (Springer) p. 434

[22] Belghachem N, Mlynczak J, Kopczynski K, Mierczyk Z and Gawron M 2016 *Optical Materials* **60** 546

[23] Galbraith J 2014 *Photoelastic Properties of Oxide and Non-oxide Glasses*, PhD Dissertation (Halifax: Dalhousie University)

[24] Tropf W J, Thomas M E and Harris T J 1995 *Properties of Crystals and Glasses, Handbook of Optics* **2** 33

[25] Graham E K and Bradt R C 1985 *Residual Stresses and Elastic Properties in Polycrystalline Materials* (Pennsylvania State University Park)

[26] Slezak O, Lucianetti A, Divoky M, Sawicka M and Mocek T 2013 *IEEE Journal of Quantum Electronics* **49** 960

[27] Bermudez J C, Pinto-Robledo V J, Kir'yanov A V and Damzen M J 2002 *Optics Communications* **210** 75

[28] Sennaroglu A 2000 *Journal of Physics D: Applied Physics* **33** 1478

[29] Fan T Y 1990 *IEEE Journal of Quantum Electronics* **26** 311

[30] Lan Y P, Chen Y F and Wang S C 2000 *Applied Physics B* **71** 27

[31] Degnan J J 1989 *IEEE Journal of Quantum Electronics* **25** 214

[32] Huang X S 2016 *Research on Diode-pumped Passively Q-switched Nd:YAG/Cr^{4+}:YAG Microchip Laser*, MS Dissertation (Beijing: Beijing university of technology) (in Chinese)

[33] Ryabtsev G I, Bezyazychnaya T V, Bogdanovich M V, Grigor'ev A V, Kabanov V V, Lebiadok Y V, Ryabtsev A G and Shchemelev M A 2012 *Applied Physics B* **108** 283